Repurposing an Ancient Protein Core Structure: Structural Studies on FmtA, a Novel Esterase of *Staphylococcus aureus*

Vikram Dalal [1], Pramod Kumar [1], Gaddy Rakhaminov [2], Aneela Qamar [2], Xin Fan [2], Howard Hunter [2], Shailly Tomar [1], Dasantila Golemi-Kotra [2] and Pravindra Kumar [1]

1 - Department of Biotechnology, *IIT, Roorkee, Uttrakhand-247667, India*
2 - Department of Biology, *York University, 4700 Keele Street, Toronto, Canada*

Correspondence to Dasantila Golemi-Kotra and Pravindra Kumar: *dgkotra@yorku.ca, kumarfbs@iitr.ac.in*
https://doi.org/10.1016/j.jmb.2019.06.019
Edited by Dan Tawfik

Abstract

FmtA is a penicillin-recognizing protein (PRP) with novel hydrolytic activity toward the ester bond between D-Ala and the backbone of teichoic acids. Teichoic acids are polyol-phosphate polymers found in the *Staphylococcus aureus* cell wall, and they play important roles in antibiotic resistance and pathogenesis. Two of the PRPs conserved motifs, namely, SXXK and Y(S)XN, are involved in the hydrolysis by FmtA, but the catalytic mechanism remains elusive. Here we determined the crystal structure of FmtA. FmtA shares the core structure of PRPs: an all α-helical domain and α/β domain sandwiched together. However, it does not have the typical PRPs active-site cleft. Its active site is shallow, solvent-exposed, and enlarged. Furthermore, our mutagenesis and kinetic studies suggest that the SXXK and Y(S)XN motifs of FmtA offer all that is necessary for catalysis, and more: the active-site nucleophile (serine), the general base (lysine) required for the acylation step and the deacylation step, and an anchor (tyrosine) to hold the active-site serine, and possibly the substrate, in an optimum conformation for catalysis. Our study establishes that the FmtA esterase activity represents an expansion of the catalytic activity repertoire of the PRPs core structure, which typically displays peptidase activity. This finding points toward a novel mechanism of ester bond hydrolysis by a PRP. The structure of FmtA provides insights to the design of inhibitor molecules with the potential to serve as leads in the development of novel antibacterial chemotherapeutic agents.

Introduction

Three decades ago, Haas and co-workers [1] proposed that the alanyl turnover of *Staphylococcus aureus* teichoic acids ought to be enzymatically driven due to its fast kinetics in intact cells ($t_{1/2}$ = 37 min, the base-catalyzed reaction has a $t_{1/2}$ = 12.5 h, at pH 7 and at 37 °C). We recently discovered that the *S. aureus* protein FmtA hydrolyzes the ester bond between D-Ala and the backbone of teichoic acids and proposed that the alanyl turnover is catalyzed by FmtA ($t_{1/2}$ = 32 min in pH 7.2 buffer, at 25 °C) [2]. This activity is unique to FmtA as no other penicillin-binding proteins (PBPs) of *S. aureus,* such as PBP4 and PBP2a, exhibited such activity [2]. Teichoic acids of *S. aureus* are poly-ribitol or -glycerolphosphate polymers attached to either the cell wall peptidoglycan or to the outer leaflet of the cytoplasmic membrane, respectively (Fig. 1) [3,4]. The former polymers are referred to as wall teichoic acids (WTA) and the latter as lipoteichoic acids (LTA). Both polymers have their backbones post-synthetically glycosylated by *N*-acetyl glucosamine (GlcNAc) or esterified by D-alanine [4,5]. The latter modification adds a positive charge to the otherwise negatively charged polyol-phosphate backbone of teichoic acids. Esterification of teichoic acids by D-Ala takes place extracellularly, and LTA has been considered the source of D-Ala for WTA [6]. However, there is no report on how this process occurs.

Teichoic acids play important roles in *S. aureus* physiology. They are implicated in *S. aureus* virulence [7], attachment to artificial surfaces [7], biofilm formation, cell division, cell autolysis [8,9], metal homeostasis [10], and resistance to cationic

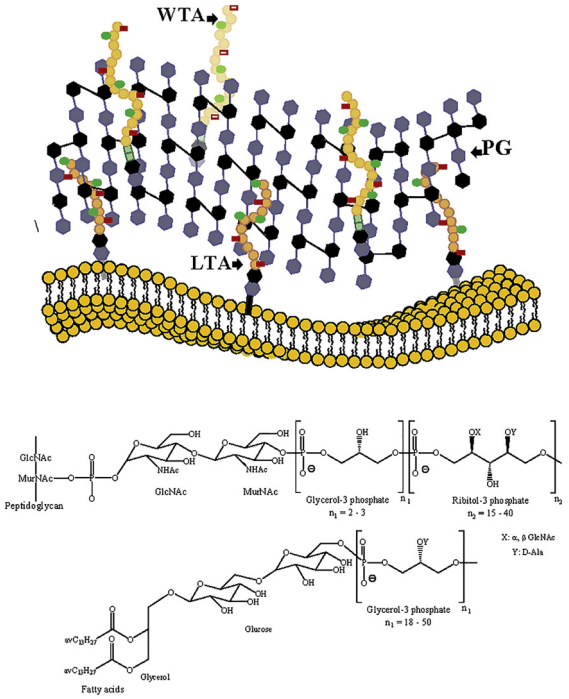

Fig. 1. A schematic view of the *S. aureus* cell surface (top panel). Highlighted are the cytoplasmic membrane, peptidoglycan (PG), lipoteichoic acid (LTA), and wall teichoic acid (WTA). D-Ala attached on teichoic acids is represented by a green circular shape, and GlnNAc is represented by a red rectangular shape. The bottom panel shows the general chemical structures of WTA and LTA, respectively.

antimicrobial peptides and cell wall active antibiotics [11]. These processes depend on the D-alanylation level of teichoic acids, which varies with growth conditions [11,12]. Hence, the D-amino esterase activity of FmtA is significant for these processes. Indeed, a number of reports have implicated FmtA on biofilm formation [13], cell division [2], and resistance to cell wall active antibiotics [14].

We sought to determine the crystal structure of FmtA with the purpose of elucidating the structural elements that enable the D-amino esterase activity of FmtA. The primary structure of FmtA shares similarities with serine active-site PBPs and β-lactamases, in particular the D-Ala, D-Ala-carboxypeptidase from *Streptomyces* sp. strain R61 (DDCP) and class C β-lactamases [15]. Its sequence harbors two of the three conserved motifs of PBPs and β-lactamases, namely, the SXXK and Y(S)XN motifs (where X is a variable residue). The third conserved motif of these enzymes, H(K/R)T(S)G (also known as the KTG-box), is not identified in FmtA. All three of these conserved motifs are involved in catalysis by PBPs and β-lactamases. However, FmtA does not exhibit the activities of PBPs or β-lactamases [2,15,16]. In this respect, FmtA is not an exception. Other proteins that harbor the PBP/β-lactamase conserved motifs exhibit a wide range of other activities such as D,D-endopeptidase [17], D,L-endopeptidase [18], D-amino acid amidase (DAA) [19,20], D-aminopeptidase (DAP) [21], and D-esterase [22] catalysis. This range speaks to the substrate and catalytic versatility of these enzymes [23]. All of these enzymes are members of the large family of penicillin-recognizing, active-site serine proteins (PRPs) [24,25]. The FmtA structure reported herein sheds light into the structural adaptations that have occurred in FmtA to enable binding to teichoic acids and to utilize the SXXK and Y(S)XN motifs for catalysis. Moreover, in light of FmtA function and the roles of teichoic acid D-alanylation in *S. aureus* physiology, pathogenicity, and antibiotic resistance, this FmtA structure provides a means to understand these processes.

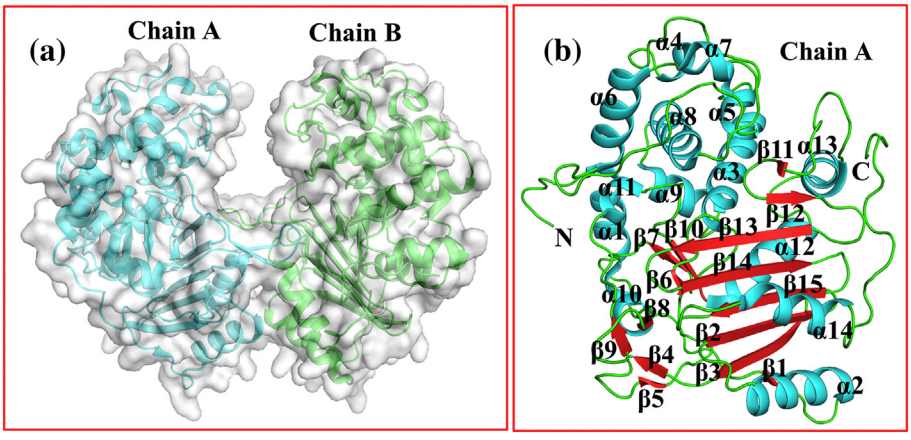

Fig. 2. FmtA structure representation: (a) A surface view (white color) and cartoon representation of the FmtA dimer: Chain A and Chain B are shown in cyan and green color, respectively. (b) The secondary structural composition of FmtA. The FmtA structure consists of 14 α-helices (cyan color), 15 β sheets (red color), and loops (green color).

Table 1. Data quality parameters of FmtA structure

PDB ID	5ZH8
Wavelength (Å)	1.5418
Resolution range (Å)	50.0–2.58 (2.62–2.58)
Space group	$C222_1$
Cell dimensions	
a, b, c (Å)	105.4, 128.2, 107.6
α, β, γ (°)	90, 90, 90
Total no. of reflections	249,309
Unique reflections	22,784
Multiplicity	3.4 (2.0)
Completeness (%)	95.7 (38)
Mean *I*/sigma(*I*)	13.28 (2.1)
CC(1/2)	0.98 (0.58)
Reflections used in refinement	21,118
Reflections used for *R*-free	1118
R_{cryst} (%)	20.8
R_{free} (%)	25.4
RMSD bonds lengths (Å)	0.005
RMSD bond angles (°)	1.03
Number of non-hydrogen atoms	5927
Macromolecules	5779
Number of protein residues	707
Ramachandran favored (%)	95.3
Ramachandran Allowed (%)	4.3
Ramachandran outliers (%)	0.4
Wilson *B*-factor (Å^2)	53.7
Average *B*-factor (Å^2)	72.0

Statistics for the highest-resolution shell are shown in parentheses.
$R_{merge} = \Sigma_{hkl}\Sigma_j | I_{hkl,j} - < I_{hkl} > | / \Sigma_{hkl}\Sigma_j | I_{hkl,j}$.

Results and Discussion

The *fmtA* gene was first identified as a factor that affects methicillin resistance in *S. aureus* two decades ago [26]. It was subsequently determined that *fmtA* is a core member of the cell wall stress stimulon in *S. aureus* [27] and a member of the VraSR regulon [28]. Fan and co-workers [15] showed, nearly a decade ago, that a FmtA construct that lacked the first 27 amino acids interacted poorly and formed covalent species with a penicillin derivative, Bocillin FL, at the serine residue of the SXXK motif. Later, these authors went on to show that FmtA interacted with teichoic acids and localized at the cell division septum [29]. Herein, we used the same protein construct (no affinity tags incorporated to the protein) to determine the FmtA crystal structure and discovered that FmtA offers novel structural features. While it harbors the core structure found in PRPs, the active site of FmtA lacks the cavity-like shape seen in these enzymes. The FmtA active site is shallow, enlarged, and fully exposed to milieu. These structural features are bound to affect binding to many of the PRPs substrates; however, they are suited for interaction with larger molecules, such as teichoic acids. In terms of the hydrolysis mechanism, the hydrogen bonding network among the conserved catalytic residues in the active site of FmtA indicates that the conserved motifs, SXXK and YND, offer the necessary elements for catalysis.

Table 2. Activities and substrate specificities of PRPs discussed in this study

PRP	Activity	Specificity[a]
DDPC	Transpeptidase, D,D-carboxypeptidase	-D-↓-D (C terminus)
DAP	Transpeptidase, amidase	(N terminus) D-↓-D(L)-
DAA	Amidase	D-↓-Amide
ADP	Endopeptidase	D-D-↓-D (L)-D(L)
EstB	Carboxylic esterase	Short aliphatic chain carboxylic esters
ClbP	Not known	Linear polyketide

[a] Arrows mark the cleavage site.

Determination of the FmtA x-ray structure

The structure of FmtA from *S. aureus* was determined by x-ray crystallography at a resolution of 2.58 Å (Fig. 2). The data were processed and indexed in the space group $C222_1$ using HKL2000 [30]. The Matthews_coeff program indicated the presence of two molecules in the asymmetric unit (namely, Chain A and Chain B) corresponding to 38% solvent content and a Mathews coefficient of 1.97 [31]. Molecular replacement was attempted using various homologous structures [Protein Data Bank (PDB) ID: 4GND, 4Y7P, 1HVB, 1SDE, and 1S6R, etc.] of FmtA. None of the search models let to a valid solution. However, the BALBES program provided suitable phases that had R_{cryst} and R_{free} values 45.0% and 50.3%, respectively. Different utility programs within Buccaneer and Autobuild generated the reference models. These models were screened on the basis of various parameters such as *B*-factors, coordination, and secondary structures. This strategy was used in an iterative manner, which helped in FmtA chain elongation. The final model of Chain A and Chain B of FmtA consists of 707 residues out of the 794 residues. Electron density is missing for side chains of the loop regions Glu58 to Val60 in Chain A, Glu58 to Ala61 in Chain B, and for the residues Lys204 and Tyr206 in Chain B. The crystallographic data collection and the refinement statistics are shown in Table 1.

The overall FmtA structure and its comparison with PRPs

Both FmtA chains in the crystal unit superpose on their Cα atoms (349 atoms) with an rmsd of 0.057 Å. Structurally, each FmtA chain in the dimer consists of 14 α-helices and 15 β-strands (Fig. 2B). Overall, the FmtA structure comprises an α/β region and an all α-helical region (Fig. 2B). The α/β domain

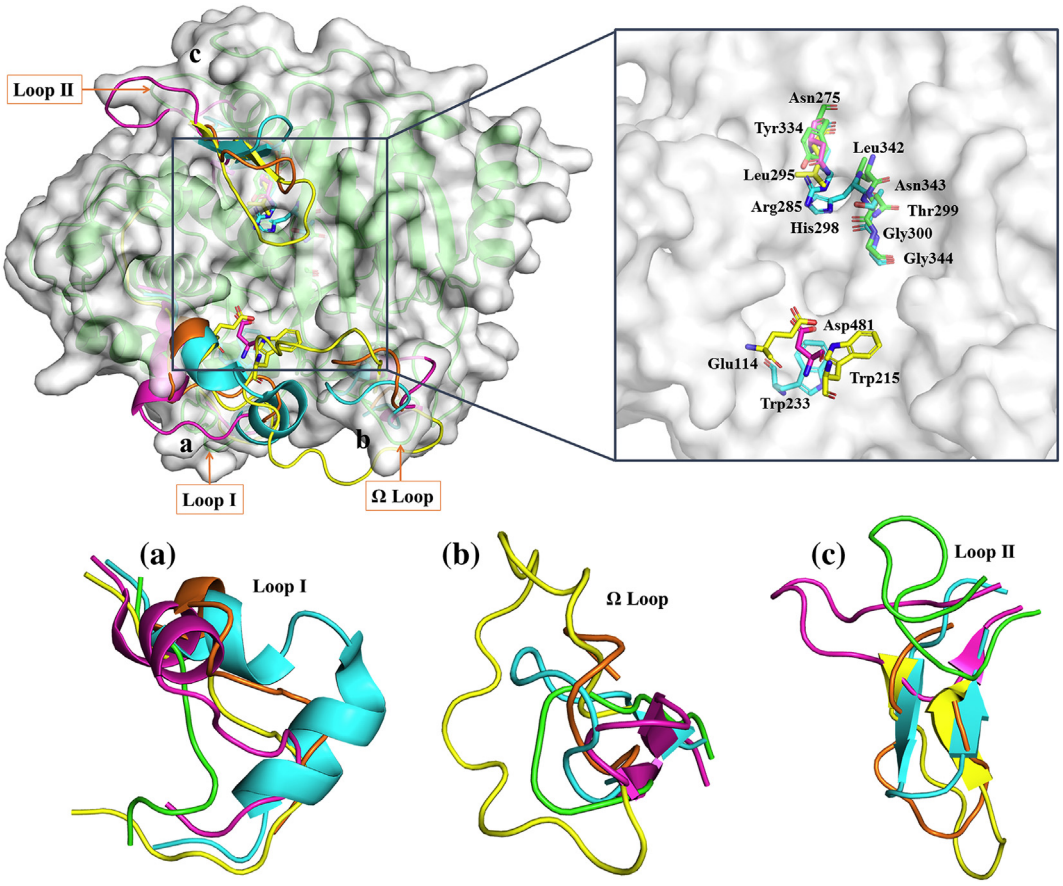

Fig. 3. A surface view and cartoon representation of FmtA, respectively, in white and green color, along with Loop I, Ω Loop, and Loop II of DDCP (cyan, PDB ID: 1PWI), DAP (pink, PDB ID: 1EI5), DAA (yellow, PDB ID: 2DNS), and ADP (orange, PDB ID: 4Y7P). The close-up view shows the FmtA active-site along with the side chains (shown in sticks) of the Leu342, Asn343, and Gly344 residues (green color); the DDCP KTG-Box residues (His298, Thr299, and Gly300 in cyan color); the Trp233 and Arg285 residues (cyan color); the residues Asn275 and Asp481 of DAP (pink color); and the residues Trp215 and Leu295 of DAA (yellow color). Panels a, b, and c highlight, respectively, the structural overlay of Loop I, Ω Loop, and Loop II regions of the above proteins.

consists of 15 β-strands forming an antiparallel β-sheet flanked by 6 α-helices, while the helical region has 8 α-helices. Dimerization between Chain A and Chain B involves three weak inter-chain hydrogen bonds (Supplementary Fig. S1). We have shown earlier that FmtA is an active monomer in solution [15]. Hence, the dimer is likely an artifact of crystallization as seen for other PRP crystal structures [22,32].

We used the DALI server to identify structural homologs of FmtA [33]. A total of 438 candidates were identified with a *Z*-score above 25. Protein structures with a *Z*-score above 31 chosen for comparison with FmtA included: DAA from *Ochrobacterum anthropic* SV3, alkaline D-peptidase (ADP) from *Bacillus cereus* DF_4-B, DAP from *O. anthropic*, AmpC β-lactamase from *Pseudomonas aeruginosa* PAO1, DDCP, carboxylesterase (EstB) from *Burkholderia gladioli*, and colibactin-maturating enzyme (ClbP) from *Escherichia coli*. These proteins are members of the PRP family of proteins (Supplementary Fig. S2). All of them have the three conserved motifs of PBPs and β-lactamases and the two domain structure folding, with the active site characteristically sandwiched between the α/β domain and the all α-helical domain, a feature known as the core structure [19,20,34]. As mentioned earlier, despite the structural similarities, these enzymes exhibit diverse activities (Table 2), although in the end, they all catalyze the cleavage of an amide bond, with the exception of the EstB, which catalyzes the hydrolysis of a carboxylic ester. The central question to be raised is as follows: which PRP structural elements are exploited to expand the catalytic function of the PRP's core structure to attain the D-amino esterase activity?

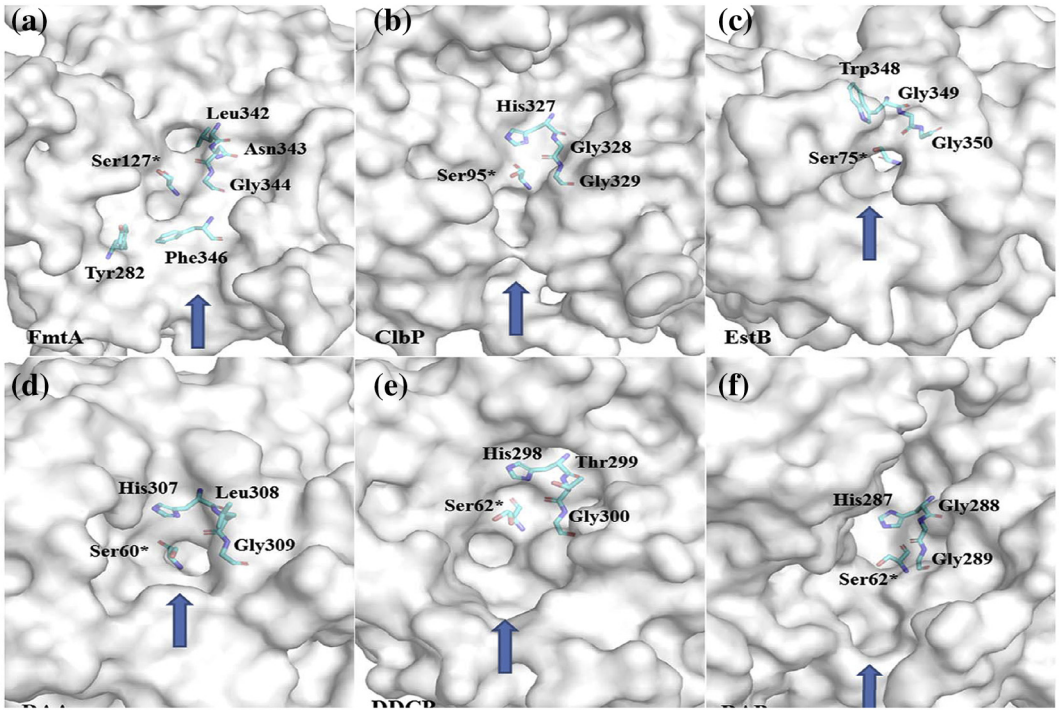

Fig. 4. Snapshots of the active-site surfaces of FmtA and PRPs: (a) FmtA, (b) ClbP (PDB ID: 3O3V), (c) EstB (PDB ID: 1CI8), (d) DAA (PDB ID: 2DNS), (e) DDCP (PDB ID: 1PW1), and (f) DAP (PDB ID: 1EI5). Nucleophilic serine and other residues that shape up substrate specificity in PRPs are shown in stick format in cyan color. The entrance to the active site in each protein is marked with an arrow.

Structural elements that shape the FmtA active site

Notwithstanding the overall structural characteristics of a member of the PRP family, FmtA lacks D, D-carboxypeptidase, β-lactamase, D-amino amidase, or D-amino peptidase activities [2]. The distinctive difference of the FmtA structure is the peripheral structural elements of the core structure, notably the loops that flank the active site. The divergence in loop sequences and conformation among structurally homologous proteins has been linked to divergence in enzyme function [35].

Three loops in particular directly impact the active site architecture (and hence function) of PRPs [19,20,34]. In FmtA, we refer to them as follows: Loop I, which extends from residues 179 to 187; Ω-Loop (as it is known in β-lactamases), which extends from residue 267 to 272; and Loop II, which extends from residue 319 to 331. Apart from the N- and C-termini, Loop I and Ω-Loop are the regions with the highest *B*-factors in FmtA (Supplementary Fig. S3). The implicit flexibility suggests a role in substrate binding. We compared these loops with those of DDCP, ADP, DAA, and DAP (Fig. 3). Loop I in FmtA connects the α5 and α6 helices. It is the shortest of the Loops I found among the proteins listed above (ADP: 17 residues, DDCP: 21 residues, DAA: 14 residues, and DAP: 18 residues). An interesting feature of Loop I in FmtA is its four lysine residues (Lys179, Lys181, Lys184, Lys187). Residues Lys179, Lys184, and Lys187 are solvent exposed and point toward the entrance of the active site. These three lysines may engage the negatively charged backbone of teichoic acids.

The Ω-Loop in FmtA connects the α10 and α11 helices. It is similar in conformation and size to the Ω-Loops of the other proteins, with the exception of DAA, in which this loop is longer (205–227) and folds over the active site (Fig. 3). A unique feature in FmtA is the lack of interaction between Loop I and Ω-Loop. This feature creates a shallow active site with a U-shaped entrance. Two residues, Tyr282 and Phe346, which are located on the opposite sides of the base of the active site, also contribute to the shallowness of the FmtA active site. Smaller side chains at these positions would have contributed to a cavity-like active site. By contrast, in the other PRPs (except for ClbP), Loop I interacts with the Ω-Loop forming a structure at the entrance to the active site that creates a cavity-like active site (Figs. 3 and 4).

Loop II in FmtA connects the α13 helix and the β12 strand (Fig. 3). The *B*-factor for this loop is one of the lowest in the protein, suggesting that it is rigid (Supplementary Fig. S3). The conformation and length of this loop are different from the other

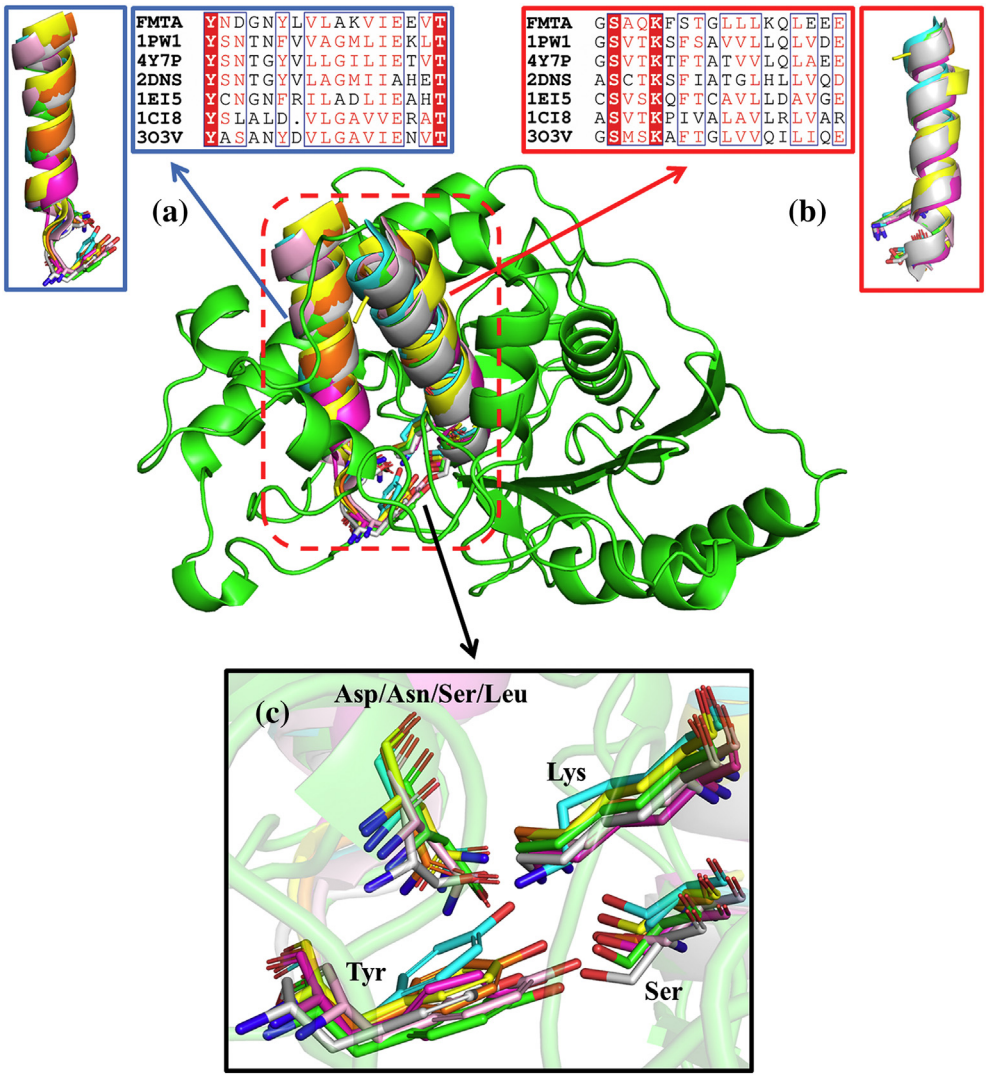

Fig. 5. The central panel is the structure (in cartoon representation) of FmtA (green color) with the overlaid conserved α3 and α8 helices of DDCP (PDB ID: 1PW1, cyan color), DAA (PDB ID: 2DNS, orange color), DAP (PDB ID: 1EI5, yellow color), ADP (PDB ID: 4Y7P, pink color), EstB (PDB ID: 1CI8, magenta color), and ClbP (PDB ID: 3O3V, gray color). The panels show: (a) the structural superposition and multiple sequence alignment of the α3 helices, (b) the structural superposition and multiple sequence alignment of the α8 helices, and (c) the overlay of the catalytic residues Ser, Lys, Tyr, and Asp in the above proteins.

PRPs. Moreover, this loop extends outward into the solution. As a result, the active site of FmtA extends along the β12 and β13 leading to its enlargement and exposure to the solvent (Fig. 3). In DDCP and DAA, Loop II is more structured (β-strand–loop–β-strand) and is tilted slightly toward the active site (Fig. 3). In addition, the orientation of this loop in these two enzymes causes the β12 and β13 strands to bend and twist toward the active site. This conformation of β12 and β13 enhances the cavity-like feature of DDCP and DAA active sites (Fig. 3). In DAP, this loop adopts a conformation and orientation that is similar to that in FmtA, but the conformation of β12 and β13 is similar to that of DDCP.

Overall, FmtA lacks four structural signatures of DDCP, ADP, DAA, DAP, and EstB: a long Loop I, interaction between Loop I and Ω-Loop, the folding of Loop II over the active site, and the tilting of the β12 and β13 strands (Fig. 3). The lack of these PRP structural signatures in FmtA contributes to the creation of a shallow, enlarged, and solvent-exposed active site (Fig. 3 and Fig. 4). Therefore, the active site of FmtA resembles that of a receptor protein binding surface, such as it would interact with a ligand protein. It is known that protein–protein interactions require a large surface area of interaction to achieve higher binding affinity [36]. It is likely that FmtA has adopted a similar strategy—a shallow, enlarged, and solvent-exposed binding surface—to

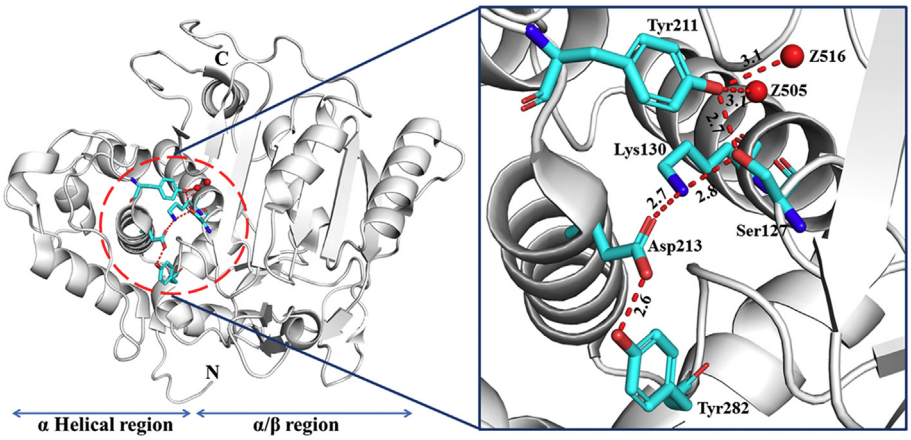

Fig. 6. Cartoon representation of the FmtA structure with the active-site residues shown in sticks. The inset panel is a close-up view of the active site. The catalytic amino acid residues and Tyr282 are shown in sticks and in cyan color. The active-site water molecules are depicted as red spheres. The hydrogen bonds among the active-site residues are depicted in red dotted lines.

bind to teichoic acids. This argument is supported by the structural similarities that exist between the active sites of FmtA and ClbP (Fig. 4). ClbP is an enzyme involved in maturation of colibactin in *E. coli*, a type of linear polyketide [34,37].

Structural elements that determine substrate specificity in FmtA

Structural studies on PRPs have reported a number of amino acids to play significant roles in substrate specificity by either guiding the substrate binding and/or defining its binding space [20,34]. For example, DAA and DAP have acquired an acidic residue in their active sites, respectively, Glu114 and Asp481, that serves as an anchor of the N-terminus of their substrates [38]. However, both these enzymes have lost the anchoring point for the C-terminus of their substrates as a result of the substitution of an arginine or tyrosine residue (Arg285 in DDCP, Tyr299 in ADP) for Leu in DAA (Leu295) or Asn in DAP (Asn275) (Fig. 3) [19,39]. These structural arrangements have led to the loss of D,D-carboxypeptidase activity and the gain of amidase activity by DAP and DAA. FmtA resembles the ADP in this respect as it carries a tyrosine residue (Tyr334) on the β12 strand. So it is unlikely that the amino group of D-Ala in teichoic acids binds to FmtA in the same way as the amino group of DAA and DAP substrates.

Additional structural features that contribute to tailoring of the binding space in PRPs are also absent in FmtA. For example, FmtA does not have the equivalents of Trp215 in DAA [20], Met480 and Ala482 [38] in DAP, or Trp 233 in DDCP [40], which are known to dictate the size of the substrate or the size of the side chains at the N-terminus or C-terminus of their substrates (Fig. 3). The absence of the above equivalent amino acids in FmtA contributes to the enlargement of the active site (Fig. 3), plausibly with a substantially reduced ability to bind the typical PRP substrates but a gain in specificity to bind teichoic acids.

This argument is strengthened by another structural feature of PRP active site. Notably, the space above and around the β13 strand is unique to each PRP and is also tailored to accommodate their specific substrates [20]. The residues on this strand, in particular those of the KTG-box, serve as a gate to the space above the β-sheet plane (Fig. 3) [20]. For example, a glycine at the second position of the KTG-box in DAP opens up the space along the β13 strand (Fig. 4), thus enabling binding of substrates with a large side chain on the amide group at their C-terminus [38]. By contrast, a leucine at this position in DAA decreases the space along the β13 strand, which leads to binding of substrates with a smaller side chain on the amide group at their C-terminus [20]. FmtA carries an asparagine at the second position in the stretch equivalent to the KTG-box. The side chain of Asn343 leads to exclusion of the space beyond the β13, and together with the side chain of Arg341 creates a wall along this strand that is likely to define binding of teichoic acid backbone along the β13 strand (Fig. 3). Thus, FmtA might have gained specificity for teichoic acids by exclusion of potentially competing substrates. The impact on the substrate specificity and enzyme activity of a bulky side chain on the β13 strand is illustrated with EstB. The sequence of the KTG-box in EstB is 348-WGG. The Trp-348 side chain is positioned above the β13 strand, and its bulkiness creates a cavity across the β-sheet plane (Fig. 4) that alters the binding mode of a cephalosporin in EstB. The impact of the altered

binding mode is the cleavage of the ester bond instead of the amide bond (the β-lactam bond) in the 7-amino cephalosporinic acid by EstB [22].

Analysis of the FmtA active site: residues responsible for catalysis

The catalytic residues in the conserved motifs SXXK and Y(S)XN in FmtA align with their homologs in DDCP, Class C β-lactamases and the PRPs presented here (Fig. 5). Hence, the conserved residues in these motifs may assume the same roles in FmtA. The SXXK motif is located at the N-terminus of the α3 helix in FmtA. The first residue in this motif (Ser127) is the proposed active-site nucleophile of FmtA. Ser127 is surrounded by a number of hydrophobic residues in FmtA (similarly to other PRPs) including Ile278, Tyr282, Ala285, and Phe346. These four amino acids, together with residues Val350 and Phe347, form the "floor" of the active site, also referred to as the hydrophobic space. The lysine in this motif (Lys130), has been assigned different catalytic roles, depending on the enzyme. In the case of DDCP and Class C β-lactamases, this residue is proposed to stabilize the oxyanion species and to reduce the pK_a of Tyr in the Y(S)XN motif [41–43]. The same lysine is also proposed to serve as the general base during acylation [44,45]. The tyrosine residue (Tyr211) in the second motif is considered to be the general base for activation of the serine nucleophile in DDCP and the deacylating water molecule in Class C β-lactamases [46]. The third residue in this motif is typically an asparagine, but it is an aspartate in FmtA (Asp213).

The KTG-box sequence is not present in FmtA. From the structural comparison studies, the sequence 342-LNG (LNG-box) of FmtA superposes with the KTG-box of DDCP. In PBPs and β-lactamases, the lysine (or histidine) of the KTG-box is involved in proton shuffling during catalysis [47]. In the case of FmtA, this position is occupied by a hydrophobic residue, Leu342. The second residue of the KTG-box is also involved in catalysis [48]. The third position of the KTG-box is always a glycine in PRPs and is notably conserved in FmtA. The conservation of this residue in PRPs is primarily to avoid steric clashes with the substrate [47]. Based on the role of the KTG-box in PRPs catalyzes, the LNG-box of FmtA is unlikely to be involved in catalysis by FmtA. Instead, the LNG sequence brings notable changes in the architecture of the FmtA active-site. The Leu342 side chain faces down the plane of the β13 strand, as does the first residue of the KTG-box in other PRPs. However, peculiarly, the Leu342 side chain is positioned away from the active site, unlike the His298 residue in DDCP, leaving the space next to Tyr211 empty and creating a pocket that is filled by a water molecule (Z505) (Figs. 3 and Fig. 6). It is likely that this pocket could accommodate the D-Ala of teichoic acid as predicted by molecular docking (see below).

In spite of the conservation of most of the PRPs catalytic residues in FmtA, there are important differences in the orientation that these residues assume and as a result the hydrogen bonding network they establish in FmtA (Fig. 6). The Tyr-211 residue is displaced by 4 Å in comparison to its homolog, Tyr159, in DDCP. This arrangement puts Tyr211 outside the boundaries of a hydrogen bond (4 Å) to Lys130, which is unusual among PRPs. However, Tyr211 remains within the hydrogen bond distance of Ser127 (2.7 Å). In addition, Tyr211 is within the hydrogen bond distance of two water molecules: Z516 and Z505 (Fig. 6), in which Z505 is within the hydrogen bond distance of Ser127. The proximity of Tyr211 to Ser127 and to at least one water molecule (Z505) may be an indication that Tyr211 could activate Ser127 as proposed in PBPs [45], and likely the water molecule Z505 as proposed in Class C β-lactamases [46]. However, both these roles require Tyr211 to be deprotonated, and there is no residue nearby that could stabilize the phenolate species of Tyr211 [41] [43]; the KTG-box in FmtA lacks a side chain with a protonated amino group, and Lys130 is not within the hydrogen bond distance of Tyr211. Notwithstanding the lack of typical amino acid residues proposed to stabilize the phenolate species of Tyr211 in PRPs, a closer look at the FmtA active site revealed an extensive hydrogen bonding network involving Tyr211; Tyr211 hydrogen bonds to Tyr329, Tyr329 to His173, His173 to Asn215, Asn215 to Ser175, and Ser175 to Leu177 amide backbone. The extensive hydrogen bonding network that Tyr211 is involved with (including Ser127 and the two water molecules) could lead to a lower pK_a of tyrosine.

The Lys-130 residue, on the other side, is well positioned to activate Ser127. It is situated within the hydrogen bond distance of Ser127 (2.8 Å) and of Asp213 (2.7 Å). Notably, Asp213 is also within the hydrogen bond distance of Tyr282 (2.6 Å), but it is 5.7 Å away from Tyr211, compared to a 2.6-Å distance seen between Asn161 and Tyr159 in DDCP. The Tyr282 residue of FmtA is unique among known PRP proteins. The hydrogen bonding network among Lys130, Asp213, and Tyr282 could stabilize the protonated state of Lys130 during catalysis through proton shuffling. A similar hydrogen bonding pattern has also been observed in EstB, a novel esterase that catalyzes the hydrolysis of short-chain aliphatic carboxylic esters [22]. EstB has a leucine residue instead of Asp213, Leu183. Notably, the side chain of a neighboring tyrosine residue, Tyr133 (located in Loop I), occupies the same space as Asp213 of FmtA and is situated within a hydrogen bond distance of a conserved water molecule. This water is within the hydrogen bond distance of an acidic residue (Asp186), three residues downstream of Leu183. Quantum

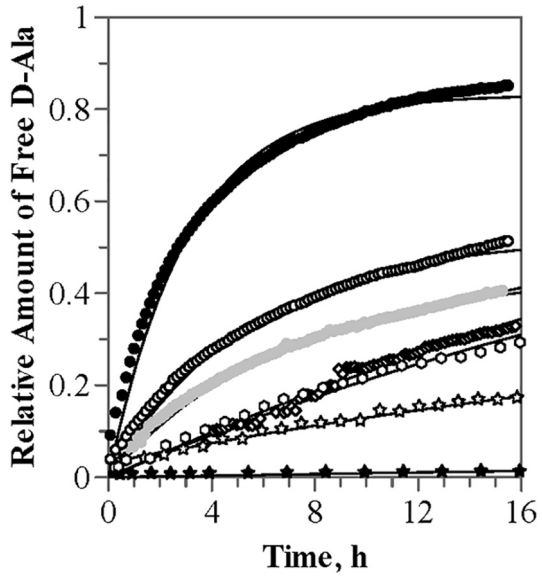

Fig. 7. The release of free D-Ala from WTA of *S. aureus* by FmtA was monitored with time by ^{1}H-NMR at 25 °C. The typical assay consisted of 10 μM of enzyme [wild-type FmtA (WT) or a FmtA variant], 5 mg/mL WTA in 50 mM sodium phosphate (pH 7.2 buffer). The data points collected for WT are represented by black solid circles [k_{obs}(WT) = 0.323 ± 0.006 h^{-1}], for the FmtATyr211Ala variant by empty circles [k_{obs}(Y211A) = 0.182 ± 0.004 h^{-1}], for the FmtAAsp213Ala variant by gray solid circles [k_{obs}(D213A) = 0.146 ± 0.003 h^{-1}], for the FmtA-Lys130ATyr211Ala variant by diamond shapes [k_{obs}(K130AY211A) = 0.0215 ± 0.004 h^{-1}], for the "isolated" *E. coli* cell extract by hexagon shapes (k_{obs} = 0.0266 h^{-1}), for the uncatalyzed reaction in 50 mM sodium phosphate (pH 7.2) by empty star shapes (k_{obs} = 0.0215 h^{-1}), and lastly for the uncatalyzed reaction in 10 mM sodium phosphate (pH 7.2) by solid star shapes (k_{obs} = 0.001 h^{-1}). The best-fitted line, for each experiment, is respectively represented by a thin line. Experimental data were fitted to a first-order rate kinetics.

mechanics and molecular mechanics calculations have shown a favorable proton transfer path from Lys78 to Tyr133, Ty133 to H_2O, and H_2O to Asp186 in EstB [49].

The hydrogen bonding network among Ser127, Lys130, and Asp213 in FmtA resembles the one seen in the catalytic triad of a typical serine protease (Ser/His/Asp) [50]. It is conceivable that in FmtA the Lys-130 residue serves as the general base for activation of Ser127 during the acylation step, and is tempting to suggest that it may also serve for activation of the water molecule during the deacylation step, although no structural water molecule was resolved in the vicinity of Lys130. However, Tyr211, positioned within hydrogen distance to Ser127, Tyr329 and Z505, may very well serve as the general base during the deacylation step, preserving in this way the function demonstrated in the case of Class C β-lactamases [43].

Roles of the PRP conserved motifs in the catalysis by FmtA

Notwithstanding the structural information on the FmtA active-site architecture and its remarkable resemblance to the Class C β-lactamases and DDCP, herein, we probed the roles of Lys130, Tyr211 and Asp213 in catalysis through mutagenesis. To the best of our knowledge, there is no similar study that has been done on the PRPs discussed herein. Hence, there is no other PRP that we can compare FmtA to when it comes to the role of the conserved motifs in the enzyme catalysis. As reported by Rahman *et al.* [2], FmtA removes D-Ala from WTA with a pseudo-first-order rate constant of 1.3 h^{-1} in 10 mM sodium phosphate, pH 7.2 buffer, at 25 °C. The uncatalyzed rate constant of D-Ala removal from WTA under identical conditions was measured to be 1 × 10^{-3} h^{-1} [2]. Hence, FmtA enhances the removal rate of D-Ala from WTA by at least 1000 fold, at 25 °C. In the same study, we reported that the substitution of Ser127 or Lys130 for Ala reduced the esterase activity of FmtA by about 84% [2]. We rationalized that the extent of reduction in the activity of each FmtA variant was in agreement with the Ser127 serving as the active-site nucleophile and Lys130 playing an important role in catalysis by FmtA. The seemingly high residual activity exhibited by these two FmtA variants could have been due to the intrinsic instability of the ester moieties in slightly acidic or basic aqueous solutions accompanied by the binding of WTA to FmtA. Enzymes are known to introduce structural constrains onto their substrates to drive them toward formation of the transition state species. Hence, it is possible that the FmtA active site may introduce enough constraints to the carbonyl carbon of the D-Ala bound to WTA to lead to its increased electrophilicity and be attacked by weak nucleophiles, such as water molecules in long incubation times—it is worth noting the two water molecules, Z516 and Z505, resolved in the structure of the FmtA active site (Fig. 6).

The FmtATyr211Ala, FmtAAsp213Ala, and FmtA-Lys130AlaTyr211Ala variants were constructed to assess the impacts of these residues on the esterase activity of FmtA. The pseudo-first-order rate constants of the D-Ala removal by FmtA and the FmtA variants in this study were measured in 50 mM sodium phosphate, pH 7.2 buffer (at 25 °C), to prevent protein aggregation under prolonged incubation times. We assessed the contribution of this buffer to the rate of D-Ala removal from WTA. The rate constant of the uncatalyzed removal of D-Ala from WTA in 50 mM sodium phosphate, pH 7.2 buffer, was determined to be 0.0215 h^{-1}, which

constitutes 5% of the FmtA activity (Fig. 7). We went so far as to also assess the possible contribution to the esterase activity of FmtA of any proteins of *E. coli* (the expression host of *fmtA*) that may co-purify with FmtA. For this purpose, *E. coli* Bl21(DE3) carrying the empty vector pET24a(+), the expression vector carrying *fmtA* (see Materials and Methods), was grown, induced and lysed exactly in the same way as if we were to isolate FmtA. The cell extract was passed through the same chromatography columns, and it was subjected through the same purification protocols as if we were purifying FmtA. The same protein-containing fractions were collected through each purification step; FmtA and its variants eluted similarly to each other in both purification steps. Lastly, the protein solution was concentrated the same way as FmtA, and we prepared the NMR sample the same way. We measured a rate constant of 0.0266 h^{-1} for the D-Ala removal in the presence of the *E. coli* cell extract. Hence, the 50 mM sodium phosphate, pH 7.2 buffer, and the "isolated" *E. coli* cell extract contributed together up to 8% of the FmtA activity under our experimental conditions (Fig. 7). These results show that the FmtA activity is highly unlikely to be due to an *E. coli* protein that may co-purify with FmtA. However, we cannot rule out completely, at this stage, the presence of an *E. coli* contaminant enzyme with low D-esterase activity in our FmtA preparations. Of note, *E. coli* does not synthesize any molecule that resembles teichoic acids. In addition, PBP4 and PBP2a of *S. aureus*, which are purified similarly to FmtA, do not exhibit D-esterase activity [2].

The FmtAAsp213Ala variant exhibited 37% of the wild-type FmtA activity, and the FmtATyr211Ala variant exhibited 48% of the wild-type FmtA activity (both corrected for the contribution of the uncatalyzed reaction) (Fig. 7). The impact of the Asp213 to Ala substitution on the FmtA activity is in agreement with the proposed role of Asp213 as a stabilizer of a neutral Lys130. The lesser impact of the Tyr211 to Ala substitution on the esterase activity of FmtA could be an indication that Lys130 may take over the role Tyr211 as a general base during deacylation—of note, Ser127 and Lys130 are within hydrogen bond distance, and moreover, due to the shallowness of the active site, it is conceivable that a water molecule from the milieu can approach the acyl-enzyme species and serve as the deacylating water molecule. However, it could also be an indication that Lys130 might serve as a general base in both steps of the FmtA-mediated catalysis, the acylation and deacylation steps, and Tyr211 may play the role of an anchor for the correct positioning of Ser127 (these residues are within hydrogen bond distance), and possibly that of WTA into the active site (see below). The latter role is in agreement with the proposed role of Tyr150 in binding the substrate in Class C β-lactamases [51].

We took a close look at the reported impacts of the equivalent amino acid substitutions on the activities of DDCP and Class C β-lactamases. In DDCP, substitution of the equivalent residue of Tyr211, Tyr159, yielded a very poorly active enzyme against peptide substrates (L-Lys–D-Ala–D-Ala) and some β-lactams, but surprisingly, the activity against nitrocefin (a cephalosporin β-lactam) or methicillin (a penicillin β-lactam) was not affected [46]. The impact of the substitution of the Asp213 homologous residue on the activity of DDCP was more complex. This residue is an asparagine in DDCP, Asn161. The substitution of Asn161 for Ala in DDCP did not have any effect on the acylation of β-lactams and thiol-ester substrates, but it had a large deleterious effect on the peptide substrates (L-Lys–D-Ala–D-Ala) [52]. In the class C β-lactamases, substitution of Tyr150 (the equivalent of Tyr211 in FmtA) also had mixed results. Dubus and co-workers [51] showed that the substitution Tyr150 for Phe in the AmpC enzyme of Class C β-lactamases had major effects on the substrate binding but not catalysis. However, Dubus and co-workers [53] showed that this substitution affected both catalysis and substrate binding. An NMR study on the pK_a value of Tyr150, showed that this residue is protonated and suggested that it is unlikely for Tyr150 to serve as the general base for activation of the active-site serine residue, Ser64 [54]. Furthermore, substitution of the Asp213 equivalent in the AmpC enzyme of the Class C β-lactamases, Asn152, had a deleterious effect on the catalysis by this enzyme [55] but not on the catalysis by the ADC-7 enzyme of the Class C β-lactamases [56]. Overall, the kinetics studies on DDCP and the Class C β-lactamases suggest that although they share the structural and the conserved motifs, they adapted differently in their use of the conserved motifs in catalysis. Moreover, within the same enzyme, the conserved motifs have adapted differently toward different substrates. Therefore, a direct comparison of the impact of the substitutions made in the FmtA conserved motifs with those made in DDCP and Class β-lactamases can be misleading.

The removal of the Lys130 and Tyr211 sidechains in the case of the FmtAK130AY211A leads to an enzyme devoid of the esterase activity (corrected for the uncatalyzed reaction). This result is 3-fold significant: first, it shows that both residues together are essential to the FmtA activity; second, there may be plasticity in catalysis in which Lys130 could replace Tyr211 in its absence, but we cannot rule out that Lys130 may serve as the sole general base in both steps of catalysis by FmtA; and lastly, the function of Tyr211 may go beyond that of a catalytic function; it could play a significant role in substrate binding (see below).

Adaptation of the PRPs core structure and the conserved motifs to the esterase activity of FmtA

While trying to reconcile the conservation of the PRPs core structure and their catalytic residues in

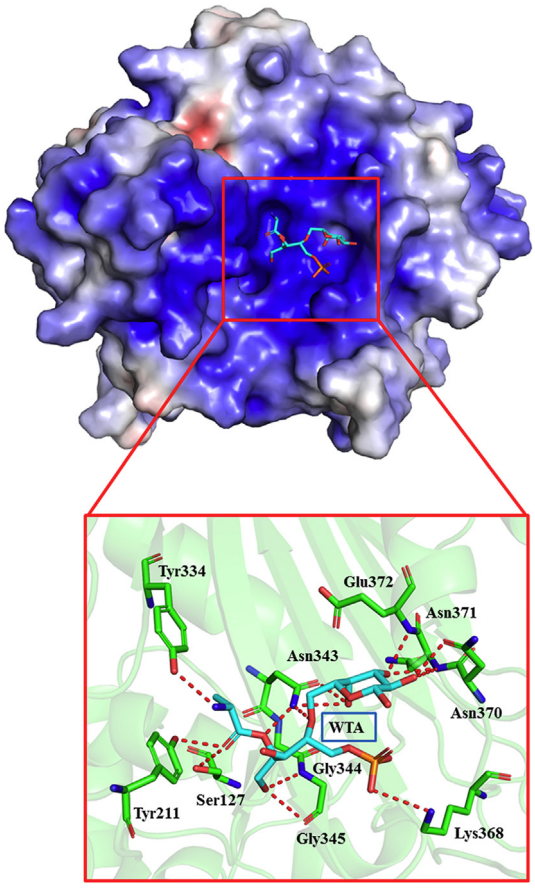

Fig. 8. Molecular docking of WTA^{mon} (shown in sticks and cyan color) on the FmtA active site (cartoon representation). The FmtA molecular surface is presented according to the electrostatic potential of FmtA. The close-up view shows the interactions of WTA with a number of FmtA amino acids (shown in sticks and green color). Hydrogen bonds are depicted in red dotted lines.

FmtA with the mechanism of catalysis by FmtA and the less-then-perfect enzymatic activity of FmtA (in terms of the rate), when comparing FmtA to Class C β-lactamases and DDCP, we raised the following questions: (a) do the residues in the PRPs conserved motifs assume a different role in the catalysis by FmtA, and (b) is their role to make a less-then-perfect enzyme. As for the former query, our structural, mutagenesis, and kinetic data (and the modeling studies below) suggest that the catalytic residues Se127, Lys130, and Asp213 are very likely to participate in de-D-alanylation of WTA in the roles proposed here. While Tyr211 may participate in catalysis in a similar role as proposed for the equivalent tyrosine residue in DDCP and Class C β–lactamases, it is likely to do so more as a vestigial catalytic element; that is, a catalytic function of Tyr211 is likely to be remnant from a predecessor enzyme, and FmtA relies on Lys130 for the deacylation step. The role of Tyr211 may be to hold Ser127 into an optimum conformation for catalysis and provide an anchor for WTA recognition, similar to the role proposed for Tyr150 in Class C β-lactamases [51]. Regarding the latter query, whether the context in which the conserved motifs are found in FmtA is such that makes FmtA a less-then-a-perfect enzyme (an enzyme that does not perform at the diffusion limit), it is worth noting that FmtA lacks a key conserved motif, the KTG-box. In all the PRPs, the Class C β-lactamases and PBPs discussed herein, the equivalent of Tyr211 is found to hydrogen bond with the lysine residue of the SXXK motif and that of the KTG-box. These interactions are considered important for the activity of Tyr211 as a general base. Hence, the loss of the KTG-box in FmtA might represent an act of enzyme evolution toward acquiring a new function, that of a D-amino esterase activity toward teichoic acids.

Implications of the kinetics of de-D-alanylation of WTA for the cell

Arguably, the rate of the D-Ala removal from WTA by FmtA is slow in comparison to the turnover rate reported for β-lactamases, which are known to perform at the diffusion limit [57]; our experiments with *E. coli* cell extract show that it is unlikely that the D-esterase activity assigned to FmtA may result from a contaminant enzyme (but we cannot rule it out completely at this stage). However, a few kinetic studies carried out with ADP and DAA show that these enzymes have rates that are similar to FmtA; The first-order rate constant of ADP against $(D\text{-}Phe)_4$ was calculated to be 0.69 h^{-1} at pH 9.0 and 30 °C [17], and that of DAP against L-Ala amide was calculated to be 0.46 h^{-1} at pH 7.0 and 30 °C [58]. The relatively slow catalytic rate by FmtA, when compared to DDCP and Class β-lactamases, could be attributed to less than optimal experimental conditions, but it could also be a reflection of the needs of the cell. It is essential that when a *S. aureus* cell is assaulted by β-lactam antibiotics, β-lactamases must efficiently and rapidly eliminate these molecules from the periplasm of the cell, as they will rapidly and permanently inhibit the PBPs. It is also equally essential that during cell division, peptidoglycan remodeling (removal of the last D-Ala from the PG precursor) and/or cross-linking of peptidoglycan must be rapid; otherwise, the growing cell may burst as a result of the high internal osmotic pressure that exists inside the cell. In the case of teichoic acids, the D-Ala content is expected to be dynamic and dependent on the environment, the growth state, and the life style of *S. aureus* (platonic *versus* growth in a biofilm) [11,12]. However, changes in the D-Ala content of teichoic acids are not expected to be drastic; that is, the complete removal of D-Ala from WTA is not expected to

Table 3. Average RMSD, RMSF, radius of gyration (Rg), solvent-accessible surface area, and intra-molecular hydrogen bonds of FmtA-native and FmtA-WTA complex

Compound	Average RMSD (Å)	Average RMSF (Å)	Average Rg (Å)	Average SASA (Å^2)	Average intra molecular hydrogen bonds numbers
FmtA-native	2.15	0.80	20.6	14,236.6	360.7
FmtA-WTA	1.79	0.79	20.5	13,872.3	368.1

happen. Studies show that the source of D-Ala on WTA is the D-Ala on LTA [6]; hence, any minor alteration on the D-Ala content is expected to be quickly readjusted. By contrast, the complete removal of D-Ala from WTA may require de novo intracellular synthesis of D-Ala [59], which may delay the refurbishing of teichoic acids with D-Ala and, as a result, the rapid re-adjustment of cells to new growth conditions. Furthermore, the expression level of *fmtA* is shown to be very low and tightly regulated under normal growth conditions [28]. This is an indication that the FmtA activity can be detrimental to the cell [16]. Therefore, as the D-Ala content is expected to be altered moderately, the kinetics of FmtA appears to be optimum for the needs of the cell.

Probing binding of WTA to FmtA through molecular docking and dynamics simulations

A single monomer of WTA (WTA^{mon}) was docked successfully into the active site of FmtA (Fig. 8). The best binding conformation was selected according to the binding score achieved from the docking process (binding energy −6.4 kcal/mol). This complex is a simplistic model of WTA binding to FmtA (as WTA is a polymer of 25 to 40 linked monomers) and is intended to represent a pre-acylation state. The electrostatic potential surface shows that the active site of FmtA is highly positive (Fig. 8), and as such, it complements well the negatively charged backbone of WTA. The predicted interactions between WTA^{mon} and FmtA are depicted in Fig. 8. In particular, the carbonyl O of D-Ala is within a hydrogen bond distance of the OH groups of Tyr211 and Ser127. The predicted interaction between Try211 and the carbonyl O of D-Ala may be an indication of Tyr211 serving to position the carbonyl moiety of D-Ala for catalysis. In addition, the amino group of D-Ala is predicted to interact with the OH groups of Tyr334 and Tyr211, which may also serve as the anchoring points for this group. The pocket in the active site created by the unique orientation of Leu-342 side chain is predicted to nestle the methyl group of D-Ala. The proposed binding mode of WTA^{mon} indicates that the water molecule Z516 might be displaced upon binding of teichoic acids to the active site, but not Z505; thus, Z516 may be unavailable for catalysis.

The molecular dynamics (MD) simulations on apoFmtA and the FmtA-WTA^{mon} complex probed the structural and conformational changes that may occur in FmtA during binding with WTA. An overlap of the snapshots of the FmtA-WTA^{mon} complex before and after the MD simulations shows that key interactions between WTA^{mon} and FmtA (highlighted above) remain stable throughout the MD simulations (Supplementary Fig. S4 and S5). The parameters such as rmsd (root means square deviation), rmsf (root means square fluctuation), and hydrogen bond formation were monitored during MD simulations of apoFmtA and the complex to assess the stability of the complex and the impact of the WTA^{mon} binding to FmtA. The analyses of these parameters revealed that binding to WTA^{mon} did not introduce major changes to FmtA. On the contrary, binding stabilized the protein (Supplementary Figs. S6, S7, and S8). On average, seven additional intramolecular hydrogen bonds were predicted to form in the protein in the case of FmtA-WTA^{mon} complex (Supplementary Fig. S7 and Table 3). Also, the intermolecular hydrogen bonds in the complex (on average six bonds) were stable throughout the MD simulations (Supplementary Fig. S8). We looked closely at the rmsf data to analyze the behavior of the flexible regions upon WTA binding—generally, loosely organized loops in a protein show higher rmsf and secondary structures show low rmsf values. In particular, Loop I (regions 178 to 190) becomes less flexible and Ω-Loop (regions 262 to 272) gains more flexibility (Supplementary Fig. S9) in the complex, suggesting that they are likely to be involved in interaction with WTA.

In conclusion, FmtA is a novel D-amino esterase [2]. Its crystal structure provides, for the first time, a close-up view of the active site and insights to the catalytic hydrolysis. The FmtA structure shares the core structure of PRPs, in which the all α-helical domain and the α/β domain are sandwiched together to form the active site. A characteristic feature of many PRPs is a deep-pocket-like active site. In addition, for many of them, the substrate specificity and the gain in function have been achieved through specific residues that reach into the active site and modulate its hydrophobic space. However, the active site of FmtA is unique among the listed PRPs; it is shallow, wide, and solvent-exposed, and

it lacks the residues that determine the substrate specificity and modulate the activity in the other PRPs. These structural features are likely to contribute to a substantially reduced ability of FmtA to bind to typical PRP substrates (as indicated by lack of many of the PRPs activities [2]), and yet provide specific recognition for teichoic acids. Furthermore, these unique structural features of the FmtA active site have been achieved primarily through the remodeling of two loops, Loop I and Loop II (Fig. 3). In terms of the hydrolysis mechanism, the novelty in catalysis by FmtA stems from adopting two of the PRPs conserved motifs, SXXK and YND, to hydrolyze an ester bond. The hydrogen bonding network observed in the FmtA crystal structure suggests that Lys130 may serve as the general base for the activation of Ser127, and Tyr211 may serve as the general base for activation of the deacylating water molecule. However, the mutagenesis and kinetic studies suggest that FmtA may rely on Lys130 as the general base for both steps of the catalysis. In addition, the kinetic studies together with the hydrogen bonding network observed in the structure of the FmtA active site and predicted by the molecular docking and dynamic simulation studies suggest that Tyr211 may play an essential role in holding the active-site nucleophile Ser127 and the D-Ala group of teichoic acids in optimum conformations for catalysis.

The esterase activity of FmtA establishes that the (α)/(α/β) peptidase core fold of PRPs displays a promiscuous catalytic activity [23]. In addition to the amidase activity, observed in many PRPs, these enzymes also possess the esterase activity. In the case of FmtA, the esterase activity is the predominant activity, but in PBPs, this activity is expected to be weak. Indeed, we demonstrated earlier that the typical PBPs such as PBP2a and PBP4 of *S. aureus* exhibit very weak esterase activity against teichoic acids [2]. PBPs represent some of the most ancient enzymes [44]. Our structural studies establish that the FmtA esterase activity is an example of nature repurposing an ancient core structure for a new function and substrate.

Materials and Methods

All reagents were ACS grade and purchased either from Merck-Millipore, Sigma, Fluka, or BioRad. Growth media were purchased from Himedia Laboratories (Mumbai, India) or VWR (Canada). Chromatography media and columns were purchased from GE Healthcare (Canada). Crystallization screens (Crystal Screen I and II, PEG/ion I and II, Index, Salt, and Crystal Screen Cryo) were procured from Hampton Research (USA).

Structure solution

The FmtA protein was purified as reported previously [15]. Initial crystallization trials for FmtA were conducted by using Hampton Research (Hampton Research Inc., Aliso Viejo, CA) commercial kits. Protein (30 mg/mL) in 50 mM sodium phosphate (pH 7.2 buffer) crystallized in 0.2 M NaCl, 0.1 M Tris (pH 8.5 buffer), and 25% PEG 3350 at 20 °C. Initial crystallization trials for FmtA were conducted by using Hampton Research (Hampton Research Inc.) commercial kits. Protein (30 mg/mL) in 50 mM sodium phosphate (pH 7.2 buffer) crystallized in 0.2 M NaCl, 0.1 M Tris (pH 8.5 buffer), and 25% PEG 3350 at 20 °C. The needle-shaped crystals appeared after 3 months of incubation (Supplementary Fig. S10). The protein crystal was cryoprotected in crystallization reservoir containing 20% glycerol. The crystal was diffracted at 100 K using Cu Kα radiation generated by a Bruker-Nonius Microstar H rotating-anode at the Macromolecular Crystallographic Unit facility, at the Indian Institute of Technology, Roorkee, India. The diffraction data were indexed, integrated, and scaled using the HKL2000 program module [30]. The MOLREP program of CCP4i7.0 suite was utilized employing various homologous structures of FmtA as search models, but none gave satisfactorily correct phases [60]. However, an automated MR pipeline, BALBES generated an initial FmtA model [61]. Buccaneer and Autobuild were applied consecutively to generate the models, which were then used for chain elongation of the initial model [62,63]. Phenix-refine was used for restrained atomic parameter refinement of the FmtA model [64]. COOT0.8.7 program was used for electron density map analysis and manual model building [65]. Further refinement was carried out by using noncrystallographic symmetry (NCS) and translation liberation screw (TLS) parameters of Phenix 1.12 [66]. The quality of the final model was assessed by using MolProbity [66]. The final model was analyzed, and figures were prepared in PyMOL2.0.5 [67]. The multiple sequence alignment of FmtA with DDCP, DAA, DAP, ADP, EstB, and ClbP was carried out by Clustal Omega and analyzed using ESpript3.0 [68,69]. The Dali server was utilized for the FmtA structure in comparison with other known structures.

Molecular docking

The structure of ribitol-2-D-Ala-4-Glc-5-phosphate was used as a representative of a single monomer of the WTA structure. Its chemical structure was drawn in Marvin suite17.13 (http://www.chemaxon.com/marvin/sketch/index.jsp). This chemical structure was converted into a PDB format by using OpenBabel and minimized using the Discovery Studio (DS) suite by Accelerys (San Diego, CA, USA) [70]. AutoDock

Vina 1.1.2 was utilized to dock WTA^{mon} onto the FmtA active site [71]. The residues Ser127, Lys130, Tyr211, and Asp213 were used to create the docking receptor grid with a spacing of 0.375 Å. Autogrid4 was utilized for the grid selection, and the dimensions of the box were set to 40 Å × 40 Å × 40 Å. The coordinates' center points were at $x = 14.88$, $y = 44.68$, and $z = 6.13$. The conformation with the lowest binding energy was saved and analyzed in PyMol.

Molecular dynamics

The simulation studies on both FmtA alone (apoFmtA) and FmtA-WTA^{mon} complex were performed with pmemd (particle mesh Ewald MD) in the Amber16 package with the amber force field on a Linux-based system [72]. The parameters and topology file of WTA^{mon} were generated by using the antechamber program of AmberTools 17 [73]. The calculation of the AM1-BCC charge model and GAFF force field parameters was employed using antechamber and tleap module available in AmberTools 17 [74,75]. Missing hydrogens were added, and AMBER ff14SB force field was used for the generation of parameters of apoFmtA and FmtA-WTA complex [76]. The systems were solvated using the TIP3P water model in a cubic box with a minimum distance of 30 Å from the closest atom of protein and neutralized by addition of Cl^- counterions. The systems were minimized for 1000 cycles by using the steepest descent method with a position restraint of 2.0 $kcal^{-1}$ $Å^{-2}$. The shake algorithm was used for the constraints of bonds and angles of proteins. The minimized systems were heated from 0 to 300 K in 500 ps using a Langevin thermostat. Furthermore, the systems were equilibrated for 500 ps at 300 K to obtain a stable density at constant pressure. Before the final production run, stable systems were equilibrated for 2 ns at NPT (constant composition, pressure, and temperature) at 300 K. Particle Mesh Ewald was utilized for the calculations of electrostatic interactions, and nonbonded cutoff distances was truncated at 8.0 Å. Finally, the MD production run of 100 ns with periodic boundary conditions was carried out with a time step of 2 fs at a constant pressure of 1 atm. The coordinates were written to the trajectory file every 10 ps, and in total, 10,000 frames were achieved. Analysis of MD was done by using *cpptraj* within AmbrTools 17 and VMD 1.9.1 [77,78].

Construction, purification, and characterization of the FmtA variants

Specifically, the pET24a (+):: $fmtA^{\Delta 27}$ vector was used as a template, and mutagenesis was carried out using *Pfu* Turbo DNA polymerase and the respective pair of mutagenic primers: DirY211A:5′-CAAAAAGCACATG*GCT*AACGATGGG-3′ and RevY211A:5′-CCCATCGTT*AGC*CATGTGCTTTTTG-3′, DirD213A:5′-CAAAAAG-CATATGTATAAC*GCT*GGGAATTAT TTAGTACTTG-3′ and RevD213A:5′-CAAGTAC-TAAATAATTCCC*AGC*GTTATACATAT GCTTTTTG-3′, the nucleotides that encode for the desired mutation are italicized in the sequence (the mutagenic primer pair for the K130A replacement was described previously [2]). The mutation was confirmed by DNA sequencing and electron-ionization mass spectrometry (Advanced Protein Technology Centre, Hospital for Sick Kids, Toronto, Canada). The protein variant was purified as described previously [15]. Substitution of Ala for Tyr did not have any effect on the protein secondary or tertiary structure as assessed by circular dichroism, thermal melting, and urea denaturation. The kinetics of D-Ala removal from WTA were carried out as described by Rahman *et al.* [2].

Data availability

Structure factors and atomic coordinates of FmtA were deposited in the PDB under accession code PDB 5ZH8.

Acknowledgments

V.D., P.K., and P.K. thank Macromolecular Crystallographic Unit, a Central Facility (MCU) at IIC, IIT Roorkee for purification, crystallization, data collection, and structure determination. V.D. thanks the Department of Biotechnology (DBT/2015/IIT-R/349) for financial support. G.R., A.Q., X.F., and D.G.K. were supported in part by a grant from the Canadian Institutes of Health Research (Operating Grant 93530), an Early Researcher Award from the Ontario Ministry of Economic Development and Innovation (Ontario, Canada; ER09-06-134), and Natural Sciences and Engineering Research Council of Canada (RGPIN/312200-2010).

Additional Information

Supplementary information accompanies this paper.

Appendix A. Supplementary data

Supplementary data to this article can be found online at https://doi.org/10.1016/j.jmb.2019.06.019.

Received 23 November 2018;
Received in revised form 15 June 2019;
Accepted 18 June 2019
Available online 28 June 2019

Keywords:
teichoic acids;
FmtA;
Staphylococcus aureus;
penicillin-recognizing proteins

Abbreviations used:
WTA, wall teichoic acid; LTA, lipoteichoic acid; PBP, penicillin-binding protein; DAA, D-amino acid amidase; DAP, D-aminopeptidase; PRP, penicillin-recognizing protein; ADP, alkaline D-peptidase; MD, molecular dynamics.

References

[1] R. Haas, H.U. Koch, W. Fischer, Alanyl turnover from Lipoteichoic acid to teichoic-acid in *Staphylococcus aureus*, FEMS Microbiol. Lett. 21 (1984) 27–31.
[2] M.M. Rahman, H.N. Hunter, S. Prova, V. Verma, A. Qamar, D. Golemi-Kotra, The *Staphylococcus aureus* methicillin resistance factor FmtA is a D-amino esterase that acts on teichoic acids, MBio. 7 (2015).
[3] S. Brown, J.P. Santa Maria, Jr., Walker S., Wall teichoic acids of gram-positive bacteria, Annu. Rev. Microbiol. 67 (2013) 313–336.
[4] M.G. Percy, A. Grundling, Lipoteichoic acid synthesis and function in gram-positive bacteria, Annu. Rev. Microbiol. 68 (2014) 81–100.
[5] F.C. Neuhaus, J. Baddiley, A continuum of anionic charge: structures and functions of D-alanyl-teichoic acids in gram-positive bacteria, Microbiol. Mol. Biol. Rev. 67 (2003) 686–723.
[6] N.T. Reichmann, A. Grundling, Location, synthesis and function of glycolipids and polyglycerolphosphate lipoteichoic acid in gram-positive bacteria of the phylum Firmicutes, FEMS Microbiol. Lett. 319 (2011) 97–105.
[7] E. Abachin, C. Poyart, E. Pellegrini, E. Milohanic, F. Fiedler, P. Berche, et al., Formation of D-alanyl-lipoteichoic acid is required for adhesion and virulence of *Listeria monocytogenes*, Mol. Microbiol. 43 (2002) 1–14.
[8] F. Fabretti, C. Theilacker, L. Baldassarri, Z. Kaczynski, A. Kropec, O. Holst, et al., Alanine esters of enterococcal lipoteichoic acid play a role in biofilm formation and resistance to antimicrobial peptides, Infect. Immun. 74 (2006) 4164–4171.
[9] M. Schlag, R. Biswas, B. Krismer, T. Kohler, S. Zoll, Yu Wenqi, H. Schwarz, A. Peschel, F. Götz, Role of staphylococcal wall teichoic acid in targeting the major autolysin Atl, Mol. Microbiol. 75 (2010) 864–873.
[10] T. Koprivnjak, V. Mlakar, L. Swanson, B. Fournier, A. Peschel, J.P. Weiss, Cation-induced transcriptional regulation of the dlt operon of *Staphylococcus aureus*, J. Bacteriol. 188 (2006) 3622–3630.
[11] A. Peschel, M. Otto, R.W. Jack, H. Kalbacher, G. Jung, F. Götz, Inactivation of the dlt operon in *Staphylococcus aureus* confers sensitivity to defensins, protegrins, and other antimicrobial peptides, J. Biol. Chem. 274 (1999) 8405–8410.
[12] A. Steen, E. Palumbo, M. Deghorain, P.S. Cocconcelli, J. Delcour, O.P. Kuipers, et al., Autolysis of *Lactococcus lactis* is increased upon D-alanine depletion of peptidoglycan and lipoteichoic acids, J. Bacteriol. 187 (2005) 114–124.
[13] B.R. Boles, M. Thoendel, A.J. Roth, A.R. Horswill, Identification of genes involved in polysaccharide-independent *Staphylococcus aureus* biofilm formation, PLoS One 5 (2010), e10146.
[14] M. Rajagopal, M.J. Martin, M. Santiago, W. Lee, V.N. Kos, T. Meredith, et al., Multidrug intrinsic resistance factors in *Staphylococcus aureus* identified by profiling fitness within high-diversity transposon libraries, MBio. 7 (2016).
[15] X. Fan, Y. Liu, D. Smith, L. Konermann, K.W. Siu, D. Golemi-Kotra, Diversity of penicillin-binding proteins. Resistance factor FmtA of *Staphylococcus aureus*, J. Biol. Chem. 282 (2007) 35143–35152.
[16] A. Qamar, D. Golemi-Kotra, Dual roles of FmtA in *Staphylococcus aureus* cell wall biosynthesis and autolysis, Antimicrob. Agents Chemother. 56 (2012) 3797–3805.
[17] Y. Asano, H. Ito, T. Dairi, Y. Kato, An alkaline D-stereospecific endopeptidase with beta-lactamase activity from *Bacillus cereus*, J. Biol. Chem. 271 (1996) 30256–30262.
[18] D.G. Bourne, P. Riddles, G.J. Jones, W. Smith, R.L. Blakeley, Characterisation of a gene cluster involved in bacterial degradation of the cyanobacterial toxin microcystin LR, Environ. Toxicol. 16 (2001) 523–534.
[19] M. Delmarcelle, M.C. Boursoit, P. Filee, S.L. Baurin, J.M. Frere, B. Joris, Specificity inversion of *Ochrobactrum anthropi* D-aminopeptidase to a D,D-carboxypeptidase with new penicillin binding activity by directed mutagenesis, Protein Sci. 14 (2005) 2296–2303.
[20] S. Okazaki, A. Suzuki, H. Komeda, S. Yamaguchi, Y. Asano, T. Yamane, Crystal structure and functional characterization of a D-stereospecific amino acid amidase from *Ochrobactrum anthropi* SV3, a new member of the penicillin-recognizing proteins, J. Mol. Biol. 368 (2007) 79–91.
[21] Y. Asano, A. Nakazawa, Y. Kato, K. Kondo, Properties of a novel D-stereospecific aminopeptidase from *Ochrobactrum anthropi*, J. Biol. Chem. 264 (1989) 14233–14239.
[22] U.G. Wagner, E.I. Petersen, H. Schwab, C. Kratky, EstB from *Burkholderia gladioli*: a novel esterase with a beta-lactamase fold reveals steric factors to discriminate between esterolytic and beta-lactam cleaving activity, Protein Sci. 11 (2002) 467–478.
[23] K. Steiner, H. Schwab, Recent advances in rational approaches for enzyme engineering, Comput Struct Biotechnol J. 2 (2012), e201209010.
[24] J.M. Frere, B. Joris, O. Dideberg, P. Charlier, J.M. Ghuysen, Penicillin-recognizing enzymes, Biochem. Soc. Trans. 16 (1988) 934–938.
[25] B. Joris, J.M. Ghuysen, G. Dive, A. Renard, O. Dideberg, P. Charlier, et al., The active-site-serine penicillin-recognizing enzymes as members of the *Streptomyces* R61 DD-peptidase family, Biochem. J. 250 (1988) 313–324.
[26] H. Komatsuzawa, M. Sugai, K. Ohta, T. Fujiwara, S. Nakashima, J. Suzuki, et al., Cloning and characterization of the fmt gene which affects the methicillin resistance level and autolysis in the presence of triton X-100 in methicillin-resistant *Staphylococcus aureus*, Antimicrob. Agents Chemother. 41 (1997) 2355–2361.
[27] F. McAleese, S.W. Wu, K. Sieradzki, P. Dunman, E. Murphy, S. Projan, et al., Overexpression of genes of the cell wall stimulon in clinical isolates of *Staphylococcus aureus* exhibiting vancomycin-intermediate–*S. aureus*-type resistance to vancomycin, J. Bacteriol. 188 (2006) 1120–1133.

[28] M. Kuroda, H. Kuroda, T. Oshima, F. Takeuchi, H. Mori, K. Hiramatsu, Two-component system VraSR positively modulates the regulation of cell-wall biosynthesis pathway in *Staphylococcus aureus*, Mol. Microbiol. 49 (2003) 807–821.
[29] Qamar A. Investigation of function and role of FmtA in *Staphylococcus aureus* response to antibiotic stress. Toronto2011.
[30] Z. Otwinowski, W. Minor, Processing of x-ray diffraction data collected in oscillation mode, Methods in enzymology (1997) 307–326.
[31] B.W. Matthews, Solvent content of protein crystals, J. Mol. Biol. 33 (1968) 491–497.
[32] W. Lee, M.A. McDonough, L. Kotra, Z.H. Li, N.R. Silvaggi, Y. Takeda, et al., A 1.2-A snapshot of the final step of bacterial cell wall biosynthesis, Proc. Natl. Acad. Sci. U. S. A. 98 (2001) 1427–1431.
[33] L. Holm, L.M. Laakso, Dali server update, Nucleic Acids Res. 44 (2016) W351–W355.
[34] A. Cougnoux, L. Gibold, F. Robin, D. Dubois, N. Pradel, A. Darfeuille-Michaud, et al., Analysis of structure-function relationships in the colibactin-maturating enzyme ClbP, J. Mol. Biol. 424 (2012) 203–214.
[35] L. Afriat-Jurnou, C.J. Jackson, D.S. Tawfik, Reconstructing a missing link in the evolution of a recently diverged phosphotriesterase by active-site loop remodeling, Biochemistry. 51 (2012) 6047–6055.
[36] M.C. Smith, J.E. Gestwicki, Features of protein-protein interactions that translate into potent inhibitors: topology, surface area and affinity, Expert Rev. Mol. Med. 14 (2012), e16.
[37] E.P. Balskus, Colibactin: understanding an elusive gut bacterial genotoxin, Nat. Prod. Rep. 32 (2015) 1534–1540.
[38] C. Bompard-Gilles, H. Remaut, V. Villeret, T. Prange, L. Fanuel, M. Delmarcelle, et al., Crystal structure of a D-aminopeptidase from *Ochrobactrum anthropi*, a new member of the 'penicillin-recognizing enzyme' family, Structure. 8 (2000) 971–980.
[39] C.C. Chen, O. Herzberg, Structures of the acyl-enzyme complexes of the *Staphylococcus aureus* beta-lactamase mutant Glu166Asp:Asn170Gln with benzylpenicillin and cephaloridine, Biochemistry. 40 (2001) 2351–2358.
[40] S. Nakano, S. Okazaki, E. Ishitsubo, N. Kawahara, H. Komeda, H. Tokiwa, et al., Structural and computational analysis of peptide recognition mechanism of class-C type penicillin binding protein, alkaline D-peptidase from *Bacillus cereus* DF4-B, Sci. Rep. 5 (2015) 13836.
[41] C. Oefner, A. D'Arcy, J.J. Daly, K. Gubernator, R.L. Charnas, I. Heinze, et al., Refined crystal structure of beta-lactamase from *Citrobacter freundii* indicates a mechanism for beta-lactam hydrolysis, Nature. 343 (1990) 284–288.
[42] E. Lobkovsky, E.M. Billings, P.C. Moews, J. Rahil, R.F. Pratt, J.R. Knox, Crystallographic structure of a phosphonate derivative of the *Enterobacter cloacae* P99 cephalosporinase: mechanistic interpretation of a beta-lactamase transition-state analog, Biochemistry. 33 (1994) 6762–6772.
[43] Y. Chen, A. McReynolds, B.K. Shoichet, Re-examining the role of Lys67 in class C beta-lactamase catalysis, Protein Sci. 18 (2009) 662–669.
[44] I. Massova, S. Mobashery, Kinship and diversification of bacterial penicillin-binding proteins and beta-lactamases, Antimicrob. Agents Chemother. 42 (1998) 1–17.
[45] A.P. Kuzin, H. Liu, J.A. Kelly, J.R. Knox, Binding of cephalothin and cefotaxime to D-ala–D-ala–peptidase reveals a functional basis of a natural mutation in a low-affinity penicillin-binding protein and in extended-spectrum beta-lactamases, Biochemistry. 34 (1995) 9532–9540.
[46] J.M. Wilkin, M. Jamin, C. Damblon, G.H. Zhao, B. Joris, C. Duez, et al., The mechanism of action of DD-peptidases: the role of tyrosine-159 in the Streptomyces R61 DD-peptidase, Biochem. J. 291 (Pt 2) (1993) 537–544.
[47] J.A. Kelly, A.P. Kuzin, The refined crystallographic structure of a DD-peptidase penicillin-target enzyme at 1.6 A resolution, J Mol Biol 254 (1995) 223–236.
[48] J.M. Wilkin, A. Dubus, B. Joris, J.M. Frere, The mechanism of action of DD-peptidases: the role of threonine-299 and -301 in the *Streptomyces* R61 DD-peptidase, Biochem. J. 301 (Pt 2) (1994) 477–483.
[49] L. Chen, X. Kong, Z. Liang, F. Ye, K. Yu, W. Dai, et al., Theoretical study of the mechanism of proton transfer in the esterase EstB from *Burkholderia gladioli*, J. Phys. Chem. B 115 (2011) 13019–13025.
[50] O.D. Ekici, M. Paetzel, R.E. Dalbey, Unconventional serine proteases: variations on the catalytic Ser/His/Asp triad configuration, Protein Sci. 17 (2008) 2023–2037.
[51] A. Dubus, S. Normark, M. Kania, M.G. Page, The role of tyrosine 150 in catalysis of beta-lactam hydrolysis by AmpC beta-lactamase from *Escherichia coli* investigated by site-directed mutagenesis, Biochemistry. 33 (1994) 8577–8586.
[52] J.M. Wilkin, M. Jamin, B. Joris, J.M. Frere, Mechanism of action of DD-peptidases: role of asparagine-161 in the *Streptomyces* R61 DD-peptidase, Biochem. J. 293 (Pt 1) (1993) 195–201.
[53] A. Dubus, P. Ledent, J. Lamotte-Brasseur, J.M. Frere, The roles of residues Tyr150, Glu272, and His314 in class C beta-lactamases, Proteins. 25 (1996) 473–485.
[54] Y. Kato-Toma, T. Iwashita, K. Masuda, Y. Oyama, M. Ishiguro, pKa measurements from nuclear magnetic resonance of tyrosine-150 in class C beta-lactamase, Biochem. J. 371 (2003) 175–181.
[55] A. Dubus, S. Normark, M. Kania, M.G. Page, Role of asparagine 152 in catalysis of beta-lactam hydrolysis by *Escherichia coli* AmpC beta-lactamase studied by site-directed mutagenesis, Biochemistry. 34 (1995) 7757–7764.
[56] M.J. Skalweit, M. Li, M.A. Taracila, Effect of asparagine substitutions in the YXN loop of a class C beta-lactamase of *Acinetobacter baumannii* on substrate and inhibitor kinetics, Antimicrob. Agents Chemother. 59 (2015) 1472–1477.
[57] A. Bulychev, S. Mobashery, Class C beta-lactamases operate at the diffusion limit for turnover of their preferred cephalosporin substrates, Antimicrob. Agents Chemother. 43 (1999) 1743–1746.
[58] Y. Asano, S. Yamaguchi, Dynamic kinetic resolution of amino acid amide catalyzed by D-aminopeptidase and alpha-amino-epsilon-caprolactam racemase, J. Am. Chem. Soc. 127 (2005) 7696–7697.
[59] N.T. Reichmann, C.P. Cassona, A. Grundling, Revised mechanism of D-alanine incorporation into cell wall polymers in gram-positive bacteria, Microbiol-Sgm. 159 (2013) 1868–1877.
[60] A. Vagin, A. Teplyakov, MOLREP: an automated program for molecular replacement, J. Appl. Crystallogr. 30 (1997) 1022–1025.
[61] S. Brown, Y.H. Zhang, S. Walker, A revised pathway proposed for *Staphylococcus aureus* wall teichoic acid biosynthesis based on in vitro reconstitution of the intracellular steps, Chem. Biol. 15 (2008) 12–21.
[62] K. Cowtan, The Buccaneer software for automated model building. 1. Tracing protein chains, Acta Crystallogr. D Biol. Crystallogr. 62 (2006) 1002–1011.
[63] T.C. Terwilliger, R.W. Grosse-Kunstleve, P.V. Afonine, N.W. Moriarty, P.H. Zwart, L.-W. Hung, et al., Iterative model

building, structure refinement and density modification with the PHENIX AutoBuild wizard, Acta Crystallogr. D Biol. Crystallogr. 64 (2008) 61–69.
[64] P.V. Afonine, R.W. Grosse-Kunstleve, N. Echols, J.J. Headd, N.W. Moriarty, M. Mustyakimov, et al., Towards automated crystallographic structure refinement with phenix.refine, Acta Crystallogr. D Biol. Crystallogr. 68 (2012) 352–367.
[65] P. Emsley, K. Cowtan, Coot: model-building tools for molecular graphics, Acta Crystallogr. D Biol. Crystallogr. 60 (2004) 2126–2132.
[66] P.D. Adams, P.V. Afonine, G. Bunkóczi, V.B. Chen, I.W. Davis, N. Echols, et al., PHENIX: a comprehensive Python-based system for macromolecular structure solution, Acta Crystallogr. D Biol. Crystallogr. 66 (2010) 213–221.
[67] DeLano WL. The PyMOL molecular graphics system. http://pymolorg. 2012.
[68] F. Sievers, A. Wilm, D. Dineen, T.J. Gibson, K. Karplus, W. Li, et al., Fast, scalable generation of high-quality protein multiple sequence alignments using Clustal Omega, Mol. Syst. Biol. 7 (2011) 539.
[69] P. Gouet, E. Courcelle, D.I. Stuart, F. Métoz, ESPript: analysis of multiple sequence alignments in PostScript, Bioinformatics 15 (1999) 305–308.
[70] N.M. O'Boyle, M. Banck, C.A. James, C. Morley, T. Vandermeersch, G.R. Hutchison, Open label: an open chemical toolbox, Journal of cheminformatics. 3 (2011) 33.
[71] O. Trott, A. Olson, AutoDock Vina: inproving the speed and accuracy of docking with a new scoring function, efficient optimization and multithreading, J. Comput. Chem. 31 (2010) 455–461.
[72] D.R. Roe, T.E. Cheatham, W. Humphrey, A. Dalke, K. Schulten, M.J. Abraham, et al., Automatic atom type and bond type perception in molecular mechanical calculations, J. Comput. Chem. 23 (2013) 455–461.
[73] D.A. Case, T.E. Cheatham, T. Darden, H. Gohlke, R. Luo, K. M. Merz, et al., The Amber biomolecular simulation programs, J. Comput. Chem. 26 (2005) 1668–1688.
[74] A. Jakalian, D.B. Jack, C.I. Bayly, Fast, efficient generation of high-quality atomic charges. AM1-BCC model: II. Parameterization and validation, J. Comput. Chem. 23 (2002) 1623–1641.
[75] S.K. Jain, M. Paul-Satyaseela, G. Lamichhane, K.S. Kim, W. R. Bishai, Mycobacterium tuberculosis invasion and traversal across an in vitro human blood–brain barrier as a pathogenic mechanism for central nervous system tuberculosis, J. Infect. Dis. 193 (2006) 1287–1295.
[76] J.A. Maier, C. Martinez, K. Kasavajhala, L. Wickstrom, K.E. Hauser, C. Simmerling, ff14SB: improving the accuracy of protein side chain and backbone parameters from ff99SB, J. Chem. Theory Comput. 11 (2015) 3696–3713.
[77] W. Humphrey, A. Dalke, K. Schulten, VMD: visual molecular dynamics, J. Mol. Graph. 14 (1996) 33–38.
[78] D.R. Roe, T.E. Cheatham III, PTRAJ and CPPTRAJ: software for processing and analysis of molecular dynamics trajectory data, J. Chem. Theory Comput. 9 (2013) 3084–3095.